

Article

Theoretical Study of the Efficient Ion Acceleration Driven by Petawatt-Class Lasers via Stable Radiation Pressure Acceleration

Meng Liu ^{1,2}, Jia-Xiang Gao ³, Wei-Min Wang ^{3,*}  and Yu-Tong Li ^{1,4,5,*} 

- ¹ Beijing National Laboratory for Condensed Matter Physics, Institute of Physics, CAS, Beijing 100190, China; liumeng_2021@iphy.ac.cn
- ² Department of Mathematics and Physics, North China Electric Power University, Baoding 071003, China
- ³ Beijing Key Laboratory of Opto-Electronic Functional Materials and Micro-Nano Devices, Department of Physics, Renmin University of China, Beijing 100872, China; 2020102327@ruc.edu.cn
- ⁴ School of Physical Sciences, University of Chinese Academy of Sciences, Beijing 100049, China
- ⁵ Songshan Lake Materials Laboratory, Dongguan 523808, China
- * Correspondence: weiminwang1@ruc.edu.cn (W.-M.W.); ytli@iphy.ac.cn (Y.-T.L.)

Abstract: Laser-driven radiation pressure acceleration (RPA) is one of the most promising candidates to achieve quasi-monoenergetic ion beams. In particular, many petawatt systems are under construction or in the planning phase. Here, a stable radiation pressure acceleration (SRPA) scheme is investigated, in which a circularly-polarized (CP) laser pulse illuminates a CH_2 thin foil followed by a large-scale near-critical-density (NCD) plasma. In the laser-foil interaction, a longitudinal charge-separated electric field is excited to accelerate ions together with the heating of electrons. The heating can be alleviated by the continuous replenishment of cold electrons of the NCD plasma as the laser pulse and the pre-accelerated ions enter into the NCD plasma. With the relativistically transparent propagation of the pulse in the NCD plasma, the accelerating field with large amplitude is persistent, and its propagating speed becomes relatively low, which further accelerates the pre-accelerated ions. Our particle-in-cell (PIC) simulation shows that the SRPA scheme works efficiently with the laser intensity ranging from $6.85 \times 10^{21} \text{ W cm}^{-2}$ to $4.38 \times 10^{23} \text{ W cm}^{-2}$, e.g., a well-collimated quasi-monoenergetic proton beam with peak energy $\sim 1.2 \text{ GeV}$ can be generated by a $2.74 \times 10^{22} \text{ W cm}^{-2}$ pulse, and the energy conversion efficiency from the laser pulse to the proton beam is about 16%. The QED effects have slight influence on this SRPA scheme.

Keywords: laser driven ion acceleration; radiation pressure acceleration; near-critical-density plasma



Citation: Liu, M.; Gao, J.-X.; Wang, W.-M.; Li, Y.-T. Theoretical Study of the Efficient Ion Acceleration Driven by Petawatt-Class Lasers via Stable Radiation Pressure Acceleration. *Appl. Sci.* **2022**, *12*, 2924. <https://doi.org/10.3390/app12062924>

Academic Editors: Cristian FOCSA and Jianxing Li

Received: 30 January 2022

Accepted: 2 March 2022

Published: 13 March 2022

Publisher's Note: MDPI stays neutral with regard to jurisdictional claims in published maps and institutional affiliations.



Copyright: © 2022 by the authors. Licensee MDPI, Basel, Switzerland. This article is an open access article distributed under the terms and conditions of the Creative Commons Attribution (CC BY) license (<https://creativecommons.org/licenses/by/4.0/>).

1. Introduction

Laser-driven ion accelerators are characterized by their large accelerating field gradient and have attracted significant attention over the past two decades [1–4]. Compared with conventional accelerators, laser-driven ion accelerators have a few unique features, including higher ion density and shorter bunch duration or more compact size [4,5]. These features of such novel ion sources can be applied in various prospective applications, ranging from proton radiography for cancer treatment [6] to fast ignition of nuclear fusion [7,8] and nuclear physics [9], etc. Aiming at these applications, quasi-monoenergetic ion beams with high energy are required. For instance, such ion beams can ignite compressed fuel to generate fusion energy [10]. Radiography for cancer treatment is a representative example, for which laser-driven ion beams should have an energy spread of only 1% [3,4,6]. Due to the advancements in both laser technology and targetry, a variety of schemes have been proposed and successfully achieved in recent laser-driven ion acceleration experiments [11–14]. However, although the protons can be accelerated to a cut-off energy of near 100 MeV [12,15], they are usually not monoenergetically distributed.

To achieve quasi-monoenergetic ion beams, several mechanisms have been investigated, such as collisionless shock acceleration (CSA) [16–20], radiation pressure acceleration (RPA) [21–25], and RPA-wakefiled hybrid acceleration [26]. In one of the most-investigated mechanisms, light-sail mode of RPA, the acceleration of ions to ultrahigh energies is allowed, where a nanoscale solid foil could be continuously accelerated by an ultrashort, ultraintense laser pulse under the ideal conditions [21,22,27]. With the development of a multi-petawatt-class laser system, intensities of $10^{22}\sim 10^{23}$ W cm⁻² can be reached, for which the generation of monoenergetic GeV ion beams is one of the primary applications based on light-sail mode of RPA [28]. However, this model is usually plagued by strong electron heating due to the onset of transverse instabilities [29–31] and finite spot size [32]. These effects can lead to thermal expansion of the thin foil and relativistic transparency for the ultra-intense laser. As a consequence, the charge-separated field is destroyed and the obtained ion energy spectrum has a broad energy spread. Significant efforts [33–36] have been devoted to overcoming the limitations of this mechanism to improve the ion beam qualities, such as transverse divergence, the maximum energy, and the energy spread. Most of these scenarios are still demanded to be verified in the future experiments with the developing laser technology. Therefore, how to produce high-energy monoenergetic ion beams is still an open question in both theory and experiment.

In this paper, we propose a stable radiation pressure acceleration (SRPA) scheme by using a combination target of a CH₂ thin foil and a large-scale near-critical-density (NCD) plasma. In the primary stage, an ultra-intense laser pulse with a Gaussian shape in transverse space illuminates the thin foil, and the protons of the thin foil are pre-accelerated to sub-relativistic velocities by the light-sail mode of RPA. With the help of the NCD plasma, the strong plasma heating can be obviously alleviated and thus the pre-accelerated sub-relativistic protons can stay in the cold background. In the NCD plasma, the laser pulse propagates relatively slowly due to the relativistically transparency and, hence, the speed of the longitudinal electric field of large amplitude is limited, which is the other key factor to further accelerate the sub-relativistic protons effectively. The accelerating field with limited speed, together with the alleviated plasma heating, guarantees efficient SRPA of the protons. This SRPA scheme provides a physical mechanism exploration for the planning experiments of ion acceleration at the Ti:sapphire femtosecond laser system of the Institute of Physics, Chinese Academy of Sciences, Beijing, China [37].

2. Theory and Analysis

To accomplish the stable radiation-pressure ion acceleration process, we employ a combination target consists of a solid foil and a near-critical-density plasma. An ultrashort, intense circularly polarized (CP) laser pulse is incident from the left side onto the combination target. In the stage of laser-foil interaction, we begin with some primitive theoretical analysis based on when a nanoscale solid foil is illuminated by an ultrashort laser pulse. Under ideal conditions, the obtained mean ion energy can be estimated as [38]

$$E_i = m_i c^2 \frac{\Pi^2}{2(\Pi + 1)} \quad (1)$$

where $\Pi = 2m_e n_c a_0^2 \tau c / \sum_i m_i n_i L$, c is the speed of light in vacuum, the normalized amplitude of the CP laser pulse $a_0 \simeq (I_0 \lambda^2 / 2.74 \times 10^{18} \text{ W cm}^{-2} \mu\text{m}^2)^{1/2}$, $n_c = m_e \omega^2 / 4\pi e^2$ is the critical density, ω is the angular frequency of the laser, τ is the duration of the laser pulse, L is the foil thickness, m_e is the electron mass, and m_i and n_i are the mass and the number density of the i -th ion species, respectively. For instance, in a typical simulation case discussed in the next section, we employ a 30 fs CP laser pulse at normalized amplitude $a_0 = 100$ ($I_0 \simeq 2.74 \times 10^{22}$ W cm⁻²). Here, a laser wavelength $\lambda = 1 \mu\text{m}$ is assumed and $T_0 = \lambda/c$ is the laser period. The foil is composed of carbon and hydrogen ions with $n_e = 200n_c$ and a thickness $L = 0.085\lambda$. Substituting these parameters into Equation (1), we can easily get a mean proton energy $E_p \simeq 1.35$ GeV. As a matter of fact, the RPA process is prematurely terminated as long as the target becomes transparent due to the transverse instabilities,

the target deformation, and the plasma heating [39]. Furthermore, in the intense laser interaction with the foil, the longitudinal electric field induced by charge separation travels close to the speed of light as the foil target becomes transparent. Meanwhile, the amplitude of the longitudinal electric field, which is induced by charge separation, will drop rapidly. Therefore, the obtained proton energy is much lower than the prediction by Equation (1). Our two-dimensional (2D) particle-in-cell (PIC) simulation with the above laser and target parameters results in a broad spectrum with mean proton energy $E_p \simeq 500$ MeV, which corresponds to a sub-relativistic mean proton speed $v_p \simeq 0.73c$. To date, the corresponding optimum foil thickness, and/or the proton energy scaling with the fitted laser temporal profile have been verified [40,41] by the code EPOCH [42] of particle-in-cell simulations.

To maintain an efficient RPA process, a near-critical-density (NCD) plasma is applied to suppress the plasma heating by continuously replenishing cold electrons. More importantly, a longitudinal electric field with large amplitude is excited as the ultra-intense laser pulse propagates in relativistically transparent regime. The considerable amplitude of this excited electric field can be roughly approximated by $E_{max} \approx a_0 \omega m_e c / e$ [43]. This electric field will boost the speed of the protons dramatically. For simplicity, we assume that the local accelerating field felt by the protons is $E_x(x) \sim E_{max} / 2$, the Lorentz factor of the protons $\gamma_p = 1 / (1 - v_p^2 / c^2)^{1/2}$ can be deduced from $d\gamma_p / dx \approx \pi a_0 m_e / \lambda m_p$ [26]. For $a_0 = 100$ and $v_p \simeq 0.73c$ (the corresponding $E_p \simeq 500$ MeV) obtained in the laser-foil interaction stage, the sub-relativistic protons will be accelerated rapidly to relativistic speed in tens of microns.

The necessity of a near-critical-density plasma can be analyzed by a conservative Hamiltonian of ion motion [43]. In the co-moving frame ($x' = x - \beta_x t$) with the longitudinal electric field E_x , the ion motion is governed by:

$$H(\xi, p'_i) = \gamma_\beta \left[(1 + p_i'^2)^{1/2} - p'_i \beta_x - \frac{m_e n_c a_0^2}{2 m_i n_e} \xi^2 \right] \tag{2}$$

where $\xi = x' \omega_p$ and $p'_i = p_i / m_i c$ are the normalized coordinate and momentum of the ion, the Lorentz factor $\gamma_\beta = 1 / (1 - \beta_x^2)^{1/2}$ corresponds to the normalized velocity $\beta_x = v_x / c$ of the excited longitudinal electric field, and $v_x \simeq v_{laser}$. The propagating velocity v_{laser} of the laser front can be estimated as $v_{laser} \sim \exp(-4n_e / n_{cr}) (1 - n_e / n_{cr})^{1/2} c$ and $n_{cr} \simeq (1 + 0.48 a_0^2)^{1/2} n_c$ is the relativistic critical density for CP ultra-intense laser pulses [44,45]. The equation $H(\xi, p'_i) \leq 1$ defines the region of the ions accelerating in the $\xi - p'_i$ phase space. In overdense plasma with $n_e = 2n_c$, the ion acceleration condition $H(\xi, p'_i) < 1$, as shown in Figure 1a, is satisfied for ions with $p_i / m_i c \geq 0.7$. It means that the accelerated proton with $v_p \simeq 0.73c$ is already able to enter the accelerating region for $a_0 = 100$ and $n_e = 2n_c$. The scaling law between the required ion momentum p'_i and the initial plasma density n_e are plotted by Figure 1b, which suggests that with the lower density, the more kinetic energy is required before the proton enters into the accelerating region. For instance, the plasma density n_e needs to be higher than $0.8n_c$ for the typical parameters $a_0 = 100$ and $v_p = 0.73c$.

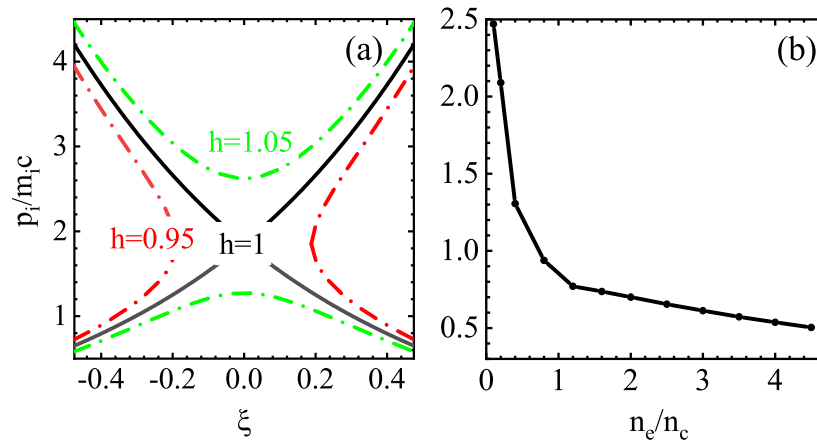


Figure 1. (a) The accelerating region of the ions in the $\xi - p'_i$ phase space with the plasma density $n_e = 2n_c$. The boundary of the accelerating region is defined by $H(\xi, p'_i) = 1$ (black solid lines) and an ion will be accelerated (red dashed lines) by the electric field if $H(\xi, p'_i) < 1$. (b) The required minimum momentum $p_i/m_i c$ as functions of the background density n_e , obtained by Equation (2). The laser normalized amplitude is taken as $a_0 = 100$.

3. Particle-In-Cell Simulation Results

To verify the efficiency of the stable-radiation-pressure ion acceleration by using a foil + NCD combination target, we carry out a series of 2D PIC simulations using the code EPOCH [42]. The circularly polarized (CP) laser pulse has a wavelength $\lambda = 1 \mu\text{m}$. Its amplitude profile is $a(t, y) = a_0 \exp(-t^2/\tau^2) \exp(-y^2/R^2)$. In typical simulations, a 30 fs laser pulse has the amplitude $a_0 = 100$ and the waist $R = 6\lambda$. The wavefront of the laser pulse arrives at the vacuum-foil interface $x = 0$ at $t = 0$. The thin foil is composed of carbon ions C^{6+} and protons H^+ in a 1:2 number ratio with $n_e = n_{H^+} + 6n_{C^{6+}} = 200n_c$. The semi-infinite NCD plasma only contains C^{6+} and e^- with a uniform density profile $n_e = 2n_c$. In each simulation, a $30 \mu\text{m} \times 44 \mu\text{m}$ simulation box moves along the x -axis at the speed of light and is divided into 3600×3520 cells. The box parameter set as $-29 \mu\text{m} \leq x \leq 1 \mu\text{m}$ in x -direction at $t = 0$. The thin solid foil in the front region ($0 \leq x \leq 0.085 \mu\text{m}$) and a semi-infinite NCD plasma at $x > 0.085 \mu\text{m}$. Each cell has 225 macro-particles in the foil region and 25 macro-particles in the semi-infinite plasma region.

Figure 2a,b display the energetic ion density distribution for the cases without and with the NCD plasma, respectively. In the laser interaction with the thin foil, although the protons in the focal spot area can be accelerated by the light-sail mode of RPA, the efficient light-sail acceleration ceases as the thin foil deforms and becomes transparent. So, as shown in Figure 2a,c, the protons are expanded to have a low density of a few n_c even in the laser propagating axis and the achieved proton energy spectrum is broad. By contrast, when the NCD plasma is adopted, the proton density is as high as $20n_c$ around the laser propagating axis at $t = 40T_0$, as shown in Figure 2b. At this time, the protons are still accelerated and they have quasi-monoenergetic spectrum with the peak of $\sim 1.2 \text{ GeV}$ (see Figure 2d), suggesting that the NCD plasma is essential to sustain a stable radiation pressure acceleration (SRPA). Meanwhile, the energy conversion efficiency from the laser pulse to the proton beam can reach up to 16% in this SRPA scheme.

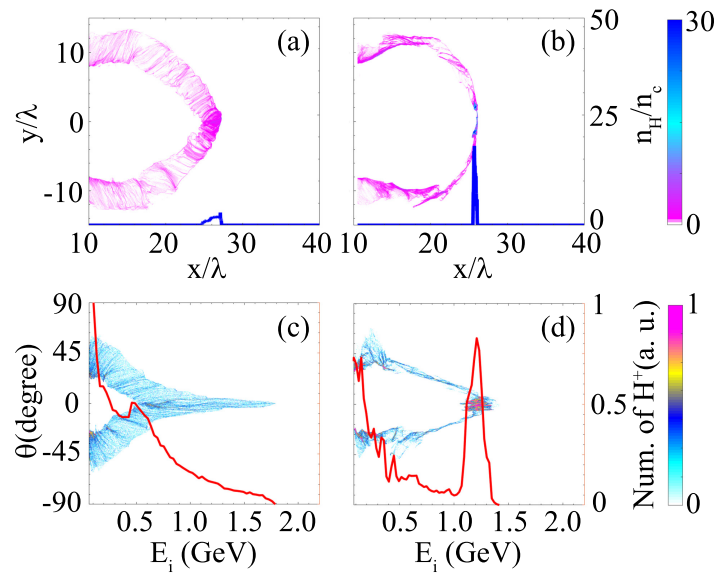


Figure 2. Comparison between different target configurations. (a,b) Proton distributions (color contour) and densities averaged at $|y| \leq 2\lambda$ (blue line) at $t = 40T_0$ obtained from the cases without and with the NCD plasma, respectively. In both cases, a CP laser pulse of $a_0 = 100$ and spot size $R = 6\lambda$ is employed. (c,d) The corresponding proton energy-angle ($\theta = \arctan(p_y/p_x$) distributions (color contour) and energy spectra (red line).

The replenishment of cold electrons in the NCD plasma plays a crucial role for suppressing the plasma heating. In Figure 3a without the NCD plasma, the plasma temperature is as high as tens of $m_e c^2$, where the plasma temperature T_e in PIC simulations is defined by the averaged kinetic energy of electrons in the center-of-momentum frame [46]. This considerable plasma heating causes the thermal expansion of the plasma and the decrease in the plasma density, which is indicated by the black and blue lines in Figure 3a. Then, the light-sail RPA process is severely disturbed and the quality of accelerated protons will also be destroyed in the later interaction period. While the NCD plasma is adopted, the plasma heating is significantly alleviated, as observed in Figure 3b. The plasma temperature is reduced by a factor of four inside the plasma peak and about halved at the laser-plasma interface. Consequently, the electrons at the laser front maintain the high density compression and, a significant number of protons (see the blue and black lines in Figure 3b) are mainly accelerated by RPA in a relatively cold plasma. Note that other ion acceleration mechanisms by virtue of the fast electrons [47–49] are suppressed.

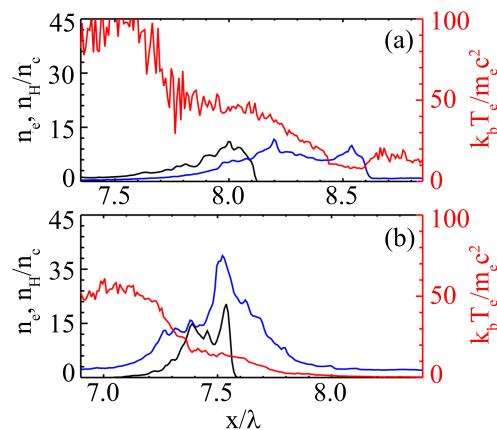


Figure 3. Plasma temperature (red line) averaged over $|y| \leq 2\lambda$ at $t = 18T_0$ for the cases (a) without and (b) with the NCD plasma, respectively. In each plot, the black and blue lines indicate the densities of the protons n_H and electrons n_e averaged over $|y| \leq 2\lambda$.

At the stage of laser foil interaction, a compressed electron layer with high density is pushed forward and a large amplitude charge-separated field is excited. Thanks to the NCD plasma, this charge-separated field can sustain a substantial amplitude and propagate at relatively low speed because the CP laser pulse of $a_0 = 100$ can propagate at around this speed in the classically overdense plasma due to relativistic transparency [44]. Figure 4a shows that the electron density peak is kept for a long time. Meanwhile, the longitudinal electric field E_x with large amplitude can be sustained, which is illustrated by Figure 4b. In addition, this longitudinal electric field is highly asymmetrical [43,50], which is characterized by a strong positive electric field at the front part and a relatively weak electric field with a negative value at the rear part. Such asymmetrical field structure is favorable for the ion acceleration.

The blue line in Figure 4c displays the temporal evolution of the propagating speed of E_x . The propagating speed is defined as the forward velocity of the longitudinal coordinate x_f , where the electric field strength peak appears. At the stage of laser-foil interaction ($t \leq 12T_0$), the propagating speed of E_x increases as long as the foil is accelerated by the RPA. At the stage of $t > 12T_0$, it is clear that the propagating speed of E_x substantially depends on the density of the NCD plasma as the thin foil becomes transparent. In the uniform NCD plasma with $n_e = 2n_c$, the propagating speed can be estimated as $v_x \simeq v_{laser} \simeq 0.88c$. The propagating speed at first remains quasi-steady at the speed of $0.87c$, then decreases gradually due to the laser depletion. Such a large amplitude longitudinal electric field with a sub-relativistic speed helps to boost the speed of a large amount of protons further. As shown by the pink triangles in Figure 4c, the speed of the proton energy peak reaches up to $0.91c$ after about $40T_0$. A track of a typical proton from the energy peak is plotted by the black dotted line in Figure 4b, which illustrates the proton is trapped in the accelerating field peak. This typical track suggests that the protons in the energy peak are accelerated by the co-moving longitudinal electric field until they surpass the accelerating field. This means a quasi-monoenergetic proton beam can be attained in this SRPA scheme. The dense quasi-monoenergetic beam can be seen in Figure 2d, which has a FWHM energy spread $\sim 13\%$ at the peak about 1.2 GeV and an opening angle $\sim 8.5^\circ$. Furthermore, the number of the proton beam can also be greatly enhanced in the case with the NCD plasma. As shown in Figure 2c,d, the number of the protons above 1 GeV in the case with the NCD plasma is 4.5 times higher than the one in the case without the NCD plasma.

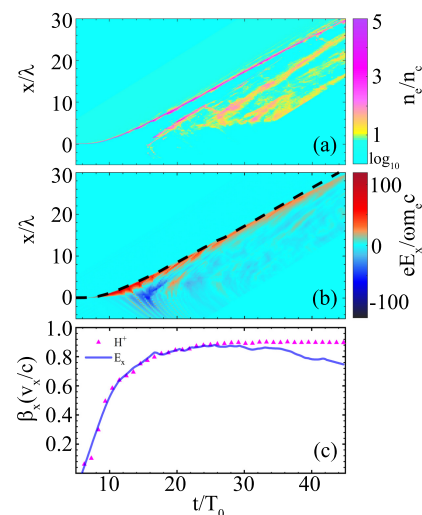


Figure 4. Temporal evolutions of (a) electron density n_e and (b) longitudinal electric field E_x . (c) Temporal evolution of the propagating velocities of the longitudinal electric field E_x (blue line) and the velocities (pink triangles) of the proton energy peak. Trajectory of a typical proton is plotted by black dotted line in (b). The simulation parameters are the same as those in Figure 2.

Our analysis in Section 2 shows that the density n_{NCD} of the NCD plasma affects the acceleration efficiency of protons. We implement a series of simulations with n_{NCD} ranging from $0.6n_c$ to $4n_c$. We find that only when $n_{NCD} > 1.2n_c$, the quasi-monoenergetic proton beam can be acquired. Figure 5a presents the dependency of the proton peak energy $E_{i,peak}$ and the corresponding energy spread η on the density n_{NCD} when the quasi-monoenergetic proton beam is generated. The peak energy $E_{i,peak}$ goes up as n_{NCD} drops and the laser propagating speed grows. In particular, the protons cannot be accelerated efficiently at $n_{NCD} > 3.5n_c$, as the protons gain a velocity around $v_p \simeq 0.73c$ at the stage of laser-foil interaction, which approaches or even exceeds the propagating speed of laser pulse and the longitudinal electric field. Note that the energy spread has an optimum value around $n_{NCD} = 2n_c$, with which the laser propagating speed is not too high or too low for the protons to easily catch up with the accelerating field and also to be further accelerated in the NCD plasma.

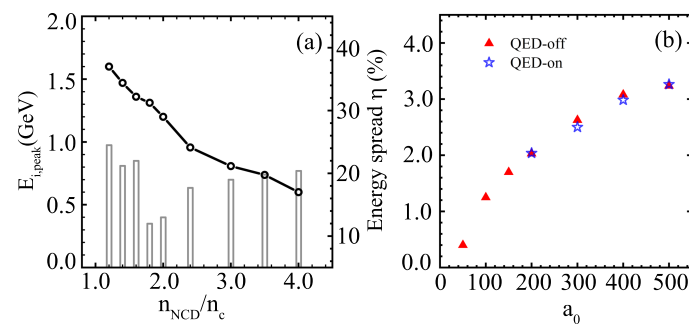


Figure 5. (a) The proton peak energy $E_{i,peak}$ (the line with circles) and the corresponding energy spread η (histograms) as a function of the initial density n_{NCD} of the NCD plasma. (b) The proton peak energy $E_{i,peak}$ as a function of the laser amplitude a_0 , where the red triangles and blue stars show the results with the QED effects switched off and switched on, respectively.

Then, we investigated the scaling law between the proton peak energy $E_{i,peak}$ and the laser amplitude a_0 , as presented by red triangles in Figure 5b. The peak energy increases rapidly as the laser amplitude ranging from $a_0 = 50$ to $a_0 = 400$. It indicates that this SRPA scheme works well at the laser intensity $I_0 \simeq 2.74 \times 10^{22} \text{ W cm}^{-2}$ and it can be extended to a larger laser intensity range. At $a_0 \geq 400$, the protons reach up to a high speed in the laser-foil interaction, while the propagating speed of the laser front and accelerating field are obviously limited in the NCD plasma. In this case, the proton acceleration in the NCD plasma is not efficient.

We also check the QED effects including photon generation via nonlinear Compton scattering and the induced radiation reaction (RR), as the laser intensity at and above $10^{23} \text{ W cm}^{-2}$ ($a_0 \geq 200$) is taken [51]. One can see from the blue stars in Figure 5b that there are no significant differences in the proton peak energies when the QED module is switched on or off. In our SRPA scheme, the high energy electrons, especially those electrons around the laser propagating axis, are mainly forward propagating along with the CP laser field. In this case, the photon generation is suppressed due to the small nonlinear quantum parameter χ_e [52,53]. In the typical simulation with $a_0 = 300$, the generated photons cover about 3% of the total laser energy.

Note that we increase the foil thickness L with the enhancement of the laser amplitude in Figure 5b. For example, we take the thickness L to 0.245λ for $a_0 = 300$ and the simulation results are presented in Figures 6 and 7. In Figure 6, one can see that the laser front moves together with the electron, proton, and carbon layers. Therefore, both the protons and ions are efficiently accelerated. From Figure 7a, one can see that the maximum momentum p_x of protons increases to $4m_i c$ at the interaction time $t = 50T_0$. The corresponding peak energy E_i of accelerated protons is about 2.5 GeV, as shown by the red line of Figure 7b. The black line of Figure 7b displays that high energy carbon ions, reaching up to 2.3 GeV/nucleus, can also be produced at the same time.

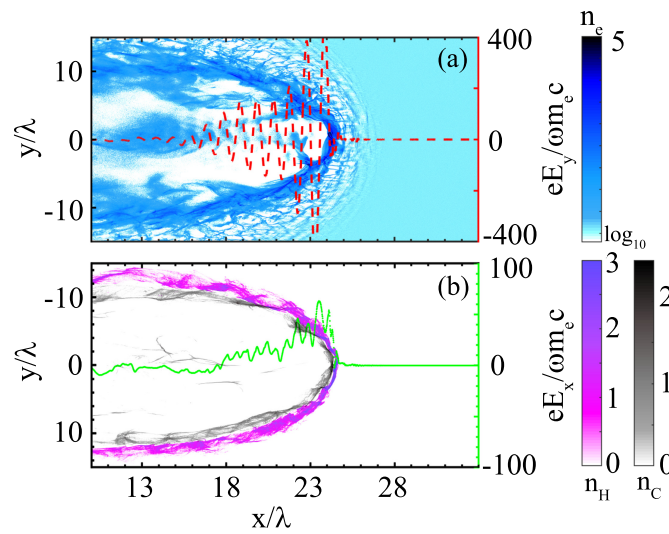


Figure 6. (a) The electron density (with the colorbar in a log scale) at $t = 35T_0$, where the laser field along the axis $y = 0$ is plotted by the red dashed line. (b) The densities of protons (n_H) and carbon ions ($n_{C^{6+}}$) with the colorbar in a log scale, where the longitudinal electric field E_x along the axis $y = 0$ is plotted by the green dotted line.

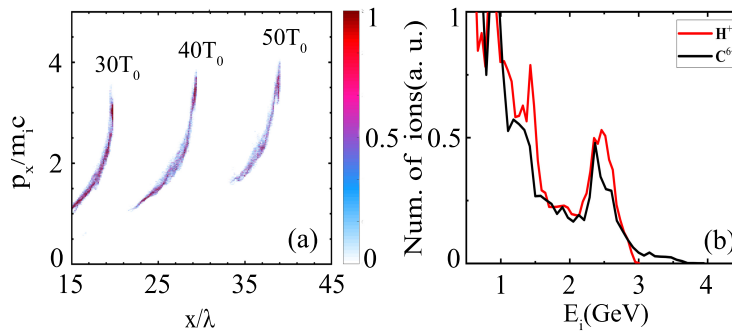


Figure 7. (a) Phase space $p_x - x$ of protons at $t = 30T_0$, $t = 40T_0$, and $t = 50T_0$, respectively. (b) Spectra of protons (red line) and carbon ions (black line) at $t = 50T_0$. Here, the laser and target parameters are the same as those in Figure 6.

4. Conclusions

It is worth pointing out that our stable radiation pressure acceleration (SRPA) scheme could provide a reference for the ion acceleration experiments with PW-class laser systems recently available and 10-PW-class laser systems available in the near future [54,55]. A NCD plasma behind the solid thin foil might be obtained by the ionization of an ultra low-density plastic foam [56]. Alternatively, such an NCD plasma might be achieved with the help of a secondary nanosecond laser pulse at a lower intensity [57].

To summarize, we have investigated, by analysis and PIC simulation, a possible stable radiation pressure acceleration (SRPA), when a multi-petawatt CP laser pulse irradiates a combination target of a CH_2 thin foil and a large-scale NCD plasma. With a suitable density range, the NCD plasma can not only significantly suppress strong electron heating in the laser-foil interaction, but also decrease the propagating speed of the laser pulse and the induced acceleration field to allow the ions to catch up. In this way, the ions can nearly co-move with the acceleration field in a relatively cold environment and, therefore, they can be efficiently accelerated. By simple analysis, a rough range of suitable NCD plasma density has been given and verified by our PIC simulation. Our simulations have shown that collimated quasi-monoenergetic proton beams with peak energy of 360 MeV and 1.2 GeV can be generated by a pulse of $a_0 = 50$ ($6.85 \times 10^{21} \text{ W cm}^{-2}$) with a $n_{NCD} = 3.5n_c$ plasma and a pulse of $a_0 = 100$ ($2.74 \times 10^{22} \text{ W cm}^{-2}$) with a $n_{NCD} = 2n_c$ plasma, respectively. The SRPA

scheme can efficiently work with the laser intensity ranging from $6.85 \times 10^{21} \text{ W cm}^{-2}$ to $4.38 \times 10^{23} \text{ W cm}^{-2}$ and the QED effects have a slight influence on this scheme.

Author Contributions: Investigation, M.L. and J.-X.G.; Supervision, W.-M.W. and Y.-T.L.; Writing—original draft, M.L. All authors have read and agreed to the published version of the manuscript.

Funding: This research received no external funding.

Institutional Review Board Statement: Not applicable.

Informed Consent Statement: Not applicable.

Data Availability Statement: Not applicable.

Acknowledgments: This work was supported by the Strategic Priority Research Program of Chinese Academy of Sciences (Grant Nos. XDA25050300, XDA25010300), the National Key R&D Program of China (Grant No. 2018YFA0404801), the National Natural Science Foundation of China (Grant Nos. 11827807) and the Fundamental Research Funds for the Central Universities (Grant Nos. 2020MS138).

Conflicts of Interest: The authors declare no conflict of interest.

References

1. Snavely, R.A.; Key, M.H.; Hatchett, S.P.; Cowan, T.E.; Roth, M.; Phillips, T.W.; Stoyer, M.A.; Henry, E.A.; Sangster, T.C.; Singh, M.S.; et al. Intense high-energy proton beams from petawatt-laser irradiation of solids. *Phys. Rev. Letts.* **2000**, *85*, 2945. [[CrossRef](#)] [[PubMed](#)]
2. Esarey, E.; Schroeder, C.B.; Leemans, W.P. Physics of laser-driven plasma-based electron accelerators. *Rev. Mod. Phys.* **2009**, *81*, 1229. [[CrossRef](#)]
3. Daido, H.; Nishiuchi, M.; Pirozhkov, A.S. Review of laser-driven ion sources and their applications. *Rep. Prog. Phys.* **2012**, *75*, 056401. [[CrossRef](#)] [[PubMed](#)]
4. Macchi, A.; Borghesi, M.; Passoni, M. Ion acceleration by superintense laser-plasma interaction. *Rev. Mod. Phys.* **2013**, *85*, 751. [[CrossRef](#)]
5. Fuchs, J.; Antici, P.; d’Humières, E.; Lefebvre, E.; Borghesi, M.; Brambrink, E.; Cecchetti, C.A.; Kaluza, M.; Malka, V.; Manclossi, M.; et al. Laser-driven proton scaling laws and new paths towards energy increase. *Nat. Phys.* **2005**, *2*, 48–54. [[CrossRef](#)]
6. Bulanov, S.V.; Esirkepov, T.Z.; Khoroshkov, V.S.; Kuznetsov, A.V.; Pegoraro, F. Oncological hadrontherapy with laser ion accelerators. *Phys. Lett. A* **2002**, *299*, 240. [[CrossRef](#)]
7. Roth, M.; Cowan, T.E.; Key, M.H.; Hatchett, S.P.; Brown, C.; Fountain, W.; Johnson, J.; Pennington, D.M.; Snavely, R.A.; Wilks, S.C.; et al. Fast ignition by intense laser-accelerated proton beams. *Phys. Rev. Letts.* **2001**, *86*, 436. [[CrossRef](#)]
8. Kitagawa, Y.; Mori, Y.; Komeda, O.; Ishii, K.; Hanayama, R.; Fujita, K.; Okihara, S. Direct heating of a laser-imploded core by ultraintense laser-driven ions *Phys. Rev. Letts.* **2015**, *114*, 195002. [[CrossRef](#)]
9. Beg, F.N.; Krushelnick, K.; Gower, C.; Torn, S.; Dangor, A.E. Table-top neutron source for characterization and calibration of dark matter detectors. *Appl. Phys. Lett.* **2002**, *80*, 3009. [[CrossRef](#)]
10. Ledingham, K.W.D.; Bolton, P.R.; Shikazono, N.; Ma, C.M.C. Towards laser driven hadron cancer radiotherapy: A review of progress. *Appl. Sci.* **2014**, *4*, 402–443. [[CrossRef](#)]
11. Wagner, F.; Deppert, O.; Brabetz, C.; Fiala, P.; Kleinschmidt, A.; Poth, P.; Schanz, V.A.; Tebartz, A.; Zielbauer, B.; Roth, M.; et al. Maximum Proton Energy above 85 MeV from the Relativistic Interaction of Laser Pulses with Micrometer Thick CH₂ Targets. *Phys. Rev. Letts.* **2016**, *116*, 205002. [[CrossRef](#)] [[PubMed](#)]
12. Kim, I.J.; Pae, K.H.; Choi, I.I.W.; Lee, C.L.; Kim, H.T.; Singhal, H.; Sung, J.H.; Lee, S.K.; Lee, H.W.; Nickles, P.V.; et al. Radiation pressure acceleration of protons to 93 MeV with circularly polarized petawatt laser pulses. *Phys. Plasmas* **2016**, *23*, 070701. [[CrossRef](#)]
13. Ma, W.J.; Kim, I.J.; Yu, J.Q.; Choi, I.W.; Singh, P.K.; Lee, H.W.; Sung, J.H.; Lee, S.K.; Lin, C.; Liao, Q.; et al. Laser acceleration of highly energetic carbon ions using a double-layer target composed of slightly underdense plasma and ultrathin foil. *Phys. Rev. Letts.* **2019**, *122*, 014803. [[CrossRef](#)] [[PubMed](#)]
14. Dover, N.P.; Nishiuchi, M.; Sakaki, H.; Kondo, K.; Alkhimova, M.A.; Faenov, A.Y.; Hata, M.; Iwata, N.; Kiriya, H.; Koga, J.K.; et al. Effect of small focus on electron heating and proton acceleration in ultrarelativistic laser-solid interactions. *Phys. Rev. Lett.* **2020**, *124*, 084802. [[CrossRef](#)]
15. Higginson, A.; Gray, R.J.; King, M.; Dance, R.J.; Williamson, S.D.R.; Butler, N.M.H.; Wilson, R.; Capdessus, R.; Armstrong, C.; Green, J.S.; et al. Near-100 MeV protons via a laser-driven transparency-enhanced hybrid acceleration scheme. *Nat. Commun.* **2018**, *9*, 724. [[CrossRef](#)]
16. Haberberger, D.; Tochitsky, S.; Fiuza, F.; Gong, C.; Fonseca, R.A.; Silva, L.O.; Mori, W.B.; Joshi, C. Collisionless shocks in laser-produced plasma generate monoenergetic high-energy proton beams. *Nat. Phys.* **2012**, *8*, 95–99. [[CrossRef](#)]

17. Liu, M.; Weng, S.M.; Li, Y.T.; Yuan, D.W.; Chen, M.; Mulser, P.; Sheng, Z.M.; Murakami, M.; Yu, L.L.; Zheng, X.L.; et al. Collisionless electrostatic shock formation and ion acceleration in intense laser interactions with near critical density plasmas. *Phys. Plasmas* **2016**, *23*, 113103. [[CrossRef](#)]
18. Chen, M.; Sheng, Z.M.; Dong, Q.L.; He, M.Q.; Li, Y.T.; Bari, M.A.; Zhang, J. Collisionless electrostatic shock generation and ion acceleration by ultraintense laser pulses in overdense plasmas. *Phys. Plasmas* **2007**, *14*, 053102. [[CrossRef](#)]
19. Chen, M.; Sheng, Z.M.; Dong, Q.L.; He, M.Q.; Weng, S.M.; Li, Y.T.; Zhang, J. Ion acceleration by colliding electrostatic shock waves in laser-solid interaction. *Phys. Plasmas* **2007**, *14*, 113106. [[CrossRef](#)]
20. Ji, L.L.; Shen, B.F.; Zhang, X.M.; Wang, F.C.; Jin, Z.Y.; Li, X.M.; Wen, M.; Cary, J.R. Generation monoenergetic heavy-ion bunches with laser-induced electrostatic shocks. *Phys. Rev. Lett.* **2008**, *101*, 164802. [[CrossRef](#)]
21. Yan, X.Q.; Lin, C.; Sheng, Z.M.; Guo, Z.Y.; Liu, B.C.; Lu, Y.R.; Fang, J.X.; Chen, J.E. Generating High-Current Monoenergetic Proton Beams by a Circularly Polarized Laser Pulse in the Phase-Stable Acceleration Regime. *Phys. Rev. Lett.* **2008**, *100*, 135003. [[CrossRef](#)] [[PubMed](#)]
22. Qiao, B.; Zepf, M.; Borghesi, M.; Geissler, M. Stable GeV Ion-Beam Acceleration from Thin Foils by Circularly Polarized Laser Pulses. *Phys. Rev. Lett.* **2009**, *102*, 145002. [[CrossRef](#)] [[PubMed](#)]
23. Chen, M.; pukhov, A.; Yu, T.P. Enhanced collimated GeV monoenergetic ion acceleration from a shaped foil target irradiated by a circularly polarized laser pulse. *Phys. Rev. Lett.* **2009**, *103*, 024801. [[CrossRef](#)] [[PubMed](#)]
24. Yu, T.P.; Pukhov, A.; Shvets, G.; Chen, M. Stable laser-driven proton beam acceleration from a two-ion-species ultrathin foil. *Phys. Rev. Lett.* **2010**, *105*, 065002. [[CrossRef](#)] [[PubMed](#)]
25. Wang, W.P.; Shen, B.F.; Xu, Z.Z. Accelerating gradient improvement from hole-boring to light-sail stage using shape-tailored laser front. *Phys. Plasmas* **2017**, *24*, 013104. [[CrossRef](#)]
26. Liu, M.; Weng, S.M.; Wang, H.C.; Chen, M.; Zhao, Q.; Sheng, Z.M.; He, M.Q.; Li, Y.T.; Zhang, J. Efficient injection of radiation-pressure-accelerated sub-relativistic protons into laser wakefield acceleration based on 10 PW lasers. *Phys. Plasmas* **2018**, *25*, 063103. [[CrossRef](#)]
27. Qiao, B.; Zepf, M.; Borghesi, M.; Dromey, B.; Geissler, M.; Karmakar, A.; Gibbon, P. Radiation-Pressure Acceleration of Ion Beams from Nanofoil Targets: The Leaky Light-Sail Regime. *Phys. Rev. Lett.* **2010**, *105*, 155002. [[CrossRef](#)]
28. Yu, T.P.; Ma, Y.Y.; Chen, M.; Shao, F.Q.; Yu, M.Y.; Gu, Y.Q.; Yin, Y. Quasimonoenergetic proton beam from ultraintense-laser irradiation of a target with holed backside. *Phys. Plasmas* **2009**, *16*, 033112. [[CrossRef](#)]
29. Pegoraro, F.; Bulanov, S.V. Photon Bubbles and Ion Acceleration in a Plasma Dominated by the Radiation Pressure of an Electromagnetic Pulse. *Phys. Rev. Lett.* **2007**, *99*, 065002. [[CrossRef](#)]
30. Palmer, C.A.J.; Schreiber, J.; Nagel, S.R.; Dover, N.P.; Bellei, C.; Beg, F.N.; Bott, S.; Clarke, R.J.; Dangor, A.E.; Hassan, S.M.; et al. Rayleigh-Taylor Instability of an Ultrathin Foil Accelerated by the Radiation Pressure of an Intense Laser. *Phys. Rev. Lett.* **2012**, *108*, 225002. [[CrossRef](#)]
31. Wan, Y.; Andriyash, I.A.; Lu, W.; Mori, W.B.; Malks, V. Effects of the Transverse Instability and Wave Breaking on the Laser-Driven Thin Foil Acceleration. *Phys. Rev. Lett.* **2020**, *125*, 104801. [[CrossRef](#)] [[PubMed](#)]
32. Dollar, F.; Zulick, C.; Thomas, A.G.R.; Chvykov, V.; Davis, J.; Kalinchenko, G.; Matsuoka, T.; McGuffey, C.; Petrov, G.M.; Willingale, L.; et al. Finite spot effects on radiation pressure acceleration from intense high-contrast laser interactions with thin targets. *Phys. Rev. Lett.* **2012**, *108*, 175005. [[CrossRef](#)] [[PubMed](#)]
33. Yu, T.P.; Pukhov, A.; Sheng, Z.M. Bright Betatronlike X Rays from Radiation Pressure Acceleration of a Mass-Limited Foil Target. *Phys. Rev. Lett.* **2013**, *110*, 045001. [[CrossRef](#)] [[PubMed](#)]
34. Shen, X.F.; Qiao, B.; Zhang, H.; Kar, S.; Zhou, C.T.; Chang, H.X.; Borghesi, M.; He, X.T. Achieving stable radiation pressure acceleration of heavy ions via successive electron replenishment from ionization of a high-Z material coating. *Phys. Rev. Lett.* **2017**, *118*, 204802. [[CrossRef](#)]
35. Wang, W.P.; Shen, B.F.; Zhang, X.M.; Ji, L.L.; Wen, M.; Xu, J.C.; Yu, Y.H.; Li, Y.L.; Xu, Z.Z. Efficient acceleration of monoenergetic proton beam by sharp front laser pulse. *Phys. Plasmas* **2011**, *18*, 013103.
36. Wang, T.H.; Khudik, V.; Shvets, G. Laser-Ion Lens and Accelerator. *Phys. Rev. Lett.* **2021**, *126*, 024801. [[CrossRef](#)]
37. Zhang, B.L.; Ma, Z.Z.; Ma, J.L.; Wu, X.J.; Ouyang, C.; Kong, D.Y.; Hong, T.S.; Wang, X.; Yang, P.D.; Chen, L.M.; et al. 1.4-mJ High Energy Terahertz Radiation from Lithium Niobates. *Laser Photonics Rev.* **2021**, *15*, 2000295. [[CrossRef](#)]
38. Macchi, A.; Veghini, S.; Liseykina, T.V.; Pegoraro, F. Radiation pressure acceleration of ultrathin foils. *New J. Phys.* **2010**, *12*, 045013. [[CrossRef](#)]
39. Paradkar, B.S.; Krishnagopal, S. Electron heating in radiation-pressure-driven proton acceleration with a circularly polarized laser. *Phys. Rev. E* **2016**, *93*, 023203. [[CrossRef](#)]
40. Lv, C.; Meng, X.H.; Wang, Z.; Cao, L.H.; Wan, F.; Liu, Q.S.; Zhang, X.H.; Zhao, B.Z. Enhanced proton acceleration via the leaky light-sail regime by laser interaction with nanofoils in strongly magnetized plasmas. *Phys. Plasmas* **2020**, *27*, 063107. [[CrossRef](#)]
41. Zhou, W.J.; Wang, W.M.; Chen, L.M. Enhanced ion acceleration in the relativistic transparent regime due to the laser rising edge. *Plasma Phys. Control. Fusion* **2021**, *63*, 035016. [[CrossRef](#)]
42. Arber, T.D.; Bennett, K.; Brady, C.S.; Lawrence-Douglas, A.; Ramsay, M.G.; Sircombe, N.J.; Gillies, P.; Evans, R.G.; Schmitz, H.; Bell, A.R.; et al. Contemporary particle-in-cell approach to laser-plasma modelling. *Plasma Phys. Control. Fusion* **2015**, *57*, 113001. [[CrossRef](#)]

43. Shorokhov, O.; Pukhov, A. Ion acceleration in overdense plasma by short laser pulse. *Laser Part. Beams* **2004**, *22*, 175–181. [[CrossRef](#)]
44. Weng, S.M.; Murakami, M.; Mulser, P.; Sheng, Z.M. Ultra-intense laser pulse propagation in plasmas: From classic hole-boring to incomplete hole-boring with relativistic transparency. *New J. Phys.* **2012**, *14*, 063026. [[CrossRef](#)]
45. [[CrossRef](#)] Weng, S.M.; Mulser, P.; Sheng, Z.M. Relativistic critical density increase and relaxation and high-power pulse propagation. *Phys. Plasmas* **2012**, *19*, 022705. [[CrossRef](#)]
46. Weng, S.M.; Liu, M.; Sheng, Z.M.; Murakami, M.; Chen, M.; Yu, L.L.; Zhang, J. Dense blocks of energetic ions driven by multi-petawatt lasers. *Sci. Rep.* **2016**, *6*, 22150. [[CrossRef](#)]
47. Chao, Y.; Cao, L.H.; Zheng, C.Y.; Liu, Z.J.; He, X.T. Enhanced Proton Acceleration from Laser Interaction with a Tailored Nanowire Target. *Appl. Sci.* **2022**, *12*, 1153. [[CrossRef](#)]
48. Wilks, S.C.; Langdon, A.B.; Cowan, T.E.; Roth, M.; Singh, M.; Hatchett, S.; Key, M.H.; Pennington, D.; MacKinnon, A.; Snavely, R.A. Energetic proton generation in ultra-intense laser-solid interactions. *Phys. Plasmas*. **2001**, *8*, 542. [[CrossRef](#)]
49. Nishihara, K.; Amitani, H.; Murakami, M.; Bulanov, S.V.; Esirkepov, T.Z. High energy ions generated by laser driven coulomb explosion of cluster. *Nucl. Instr. Meth. A* **2001**, *464*, 98–102. [[CrossRef](#)]
50. Shen, B.; Li, Y.; Yu, M.Y.; Cary, J. Bubble regime for ion acceleration in a laser-driven plasma. *Phys. Rev. E* **2007**, *76*, 055402. [[CrossRef](#)]
51. Ji, L.L.; Pukhov, A.; Shen, B.F. Ion acceleration in the ‘dragging field’ of a light-pressure-driven piston. *New J. Phys.* **2014**, *16*, 063047. [[CrossRef](#)]
52. Schwinger, J. On Gauge Invariance and Vacuum Polarization. *Phys. Rev.* **1951**, *82*, 664. [[CrossRef](#)]
53. Gu, Y.J.; Klimo, O.; Bulanov, S.V.; Weber, S. Brilliant gamma-ray beam and electron–positron pair production by enhanced attosecond pulses. *Commun. Phys.* **2018**, *1*, 93. [[CrossRef](#)]
54. Danson, C.; Haefner, C.; Bromage, J.; Butcher, T.; Chanteloup, J.C.F.; Chowdhury, E.A.; Galvanauskas, A.; Gizzi, L.A.; Hein, J.; Hillier, D.I. Petawatt and exawatt class lasers worldwide. *High Power Laser Sci. Eng.* **2019**, *7*, e54. [[CrossRef](#)]
55. Barba, S.M.; Schillaci, F.; Catalano, R.; Petringa, G.; Margarone, D.; Cirrone, G.A.P. Dosimetric Optimization of a Laser-Driven Irradiation Facility Using the G4-ELIMED Application. *Appl. Sci.* **2021**, *11*, 9823. [[CrossRef](#)]
56. Chen, S.N.; Iwawaki, T.; Morita, K.; Antici, P.; Baton, S.D.; Filippi, F.; Habara, H.; Nakatsutsumi, M.; Nicolai, P.; Nazarov, W.; et al. Density and temperature characterization of long-scale length, near-critical density controlled plasma produced from ultra-low density plastic foam. *Sci. Rep.* **2016**, *6*, 21495. [[CrossRef](#)]
57. d’Humières, E.; Antici, P.; Glesser, M.; Boeker, J.; Cardelli, F.; Chen, S.; Feugeas, J.L.; Filippi, F.; Gauthier, M.; Levy, A.; et al. Investigation of laser ion acceleration in low-density targets using exploded foils. *Plasma Phys. Control. Fusion* **2013**, *55*, 124025. [[CrossRef](#)]